Cellulose (2019) 26:3845–3857
https://doi.org/10.1007/s10570-019-02269-4

ORIGINAL RESEARCH

Nitrogen plasma surface treatment for improving polar ink adhesion on micro/nanofibrillated cellulose films

Katarina Dimic-Misic · Mirjana Kostić · Bratislav Obradović · Ana Kramar · Stevan Jovanović · Dimitrije Stepanenko · Marija Mitrović-Dankulov · Saša Lazović · Leena-Sisko Johansson · Thad Maloney · Patrick Gane

Received: 26 October 2018 / Accepted: 14 January 2019 / Published online: 26 February 2019

Abstract We find that nitrogen plasma treatment of micro/nanofibrillated cellulose films increases wettability of the surface by both liquid polar water and nonpolar hexadecane. The increased wetting effect is more pronounced in the case of polar liquid, favouring the use of plasma treated micro/nanofibrillated cellulose films as substrates for a range of inkjet printing including organic-based polar-solvent inks. The films were formed from aqueous suspensions of progressively enzymatic pretreated wood-free cellulose fibres, resulting in increased removal of amorphous species producing novel nanocellulose surfaces displaying increasing crystallinity. The mechanical properties of each film are shown to be highly dependent on the enzymatic pretreatment time. The change in surface chemistry arising from exposure to nitrogen plasma is revealed using X-ray photoelectron spectroscopy. That both polar and dispersive surface energy components become increased, as measured by contact angle, is also linked to an increase in surface roughness. The change in surface free energy is exemplified to favour the trapping of photovoltaic inks.

Keywords DBD plasma · Nitrogen plasma surface treatment · Nanocellulose films · Enzymatic nanocellulose · Printing of organic-based polar inks

K. Dimic-Misic (✉) · L.-S. Johansson · T. Maloney · P. Gane
Department of Bioproducts and Biosystems, School of Chemical Engineering, Aalto University, 00076 Aalto, Helsinki, Finland
e-mail: katarina.dimic.misic@aalto.fi

M. Kostić · A. Kramar
Faculty of Technology and Metallurgy, University of Belgrade, Karnegijeva 4, Belgrade 11000, Serbia

B. Obradović
Faculty of Physics, University of Belgrade, Studentski trg 12, Belgrade 11001, Serbia

S. Jovanović · D. Stepanenko · M. Mitrović-Dankulov · S. Lazović
Institute of Physics Belgrade, University of Belgrade, Pregrevica 118, Belgrade 11080, Serbia

Introduction and background

Sustainability is one of the key targets for industrial practice today. The related research aimed at new biobased materials derived from renewable sources, is relevant for the sustainable economy. In the bioproducts industry, micro/nanofibrillated cellulose (MNFC) has attracted attention in a number of potential applications (Hubbe et al. 2017a). It can be used in standard wood products, such as paper and boards. However, most of the benefits derived from MNFC stem from its wider uptake in a range of industrial value chains, such as biodegradable packaging films and laminates. MNFC has interesting intrinsic properties derived from large specific surface area and its

alternate regions of crystallinity. The hydroxylated surface chemistry is readily suitable for chemical modification. Films formed from MNFC are considered smart materials and studied for functional materials applications. Enzyme-treated fibres used to produce cellulose nanofibrils provide higher crystallinity in the resulting nanocellulose, as enzymes digest amorphous cellulose, which acts as the glue between crystalline cellulose regions. Direct hydrogen bonding of crystalline cellulose, therefore, gives a stronger material film. An example of an important application of MNFC is as a substrate for printed solar cells based on organic inks (Zhu et al. 2014). The surface properties of MNFC films, such as wettability by liquid, topography, chemistry, surface charge, the presence of hydrophobic and hydrophilic domains, density and conformation of functional groups, all play a crucial role in printability and barrier properties. Their ability to support controlled migration of solvent ink vehicle and chromatographic differentiation of ink components is important in the printing of inkjet printable (IP) inks, and especially for production of bio-based printed functionality in a wide range of applications, such as printed electronics and printed diagnostics (Hoeng et al. 2016; Jutila et al. 2018).

Solar panel IP photovoltaic (PV) inks contain a complex mix of materials, including the organic electron acceptor (p-type) and negative electron donor (n-type) suspended in solvent together with specific surfactant(s) intended to keep the p-type and n-type components de-mixed (Kumar and Chand 2012). Although drop-on-demand (DoD) inkjet printing is a very competitive candidate for printing PV inks on film substrates, there are limitations in respect to mutual compatibility between the surface of MNFC films and mixed polar-dispersive solvents constituting the PV ink (Singh et al. 2010; Yinhua et al. 2013). Electrolyte is highly polar, for example, and so sufficient wettability is needed by providing a polar surface, despite the parallel requirement for wettability by organic species (Schultz et al. 1977; Özkan et al. 2016). This complex polar-dispersive surface energy balance is, therefore, critical (Hansson et al. 2011).

Exposure to plasma is a convenient method to modify the surface properties of polymeric materials, while keeping their bulk properties intact, making a material better adapted for printing (Möller et al. 2010; Kramer et al. 2006; Catia et al. 2015). Furthermore, as we demonstrate, it is a convenient way to introduce desired groups onto the surface of materials (Mihailovic et al. 2011). Surface properties depend on parameters of plasma treatment such as applied electrical field energy, type of feed gas, pressure, exposure time, and reactor geometry (van de Vyver et al. 2011; Jun et al. 2008).

In this work, we modify enzyme pretreated fibre-derived MNFC film surfaces using nitrogen plasma to enhance their amphiphilic surface affinity to polar and non-polar IP PV inks. Measurements of the surface free energy, surface roughness (atomic force microscopy (AFM)) and material composition [X-ray photoelectron spectroscopy (XPS)] were used to characterise the MNFC film surface before and after plasma treatment. The affinity for IP PV ink was assessed visually after inkjet printing. We also identify a correlation between the observed change in free surface energy of the MNFC film, arising from the plasma treatment, with the effect of the enzymatic pretreatment. This is related to the level of residual crystallinity increasing as a function of progressive enzymatic pretreatment (Galagan et al. 2011; Cernakova et al. 2006; Pertile et al. 2010; Vanneste et al. 2017).

To meet the requirement of sufficient tensile strength of MNFC films for the application exemplified, the rheological properties of enzymatically pretreated MNFC fibrillar suspensions were compared with the mechanical properties of corresponding obtained films, so that rheology can be used as a predictor of film strength (Maloney 2015; Zhu et al. 2014).

Materials and methods

Preparation of MNFC

For the manufacture of short MNFC fibrils, the pulp was first washed to create the sodium form by adding sodium hydroxide to a 2 w/w% fibre suspension until the pH reached 10, and then re-washed with deionised water to a conductivity of 8.2 μS. The enzymatic treatment was performed with a commercial enzyme ECOPULP® R (Ecopulp Finland Oy), produced by a genetically modified strain of Trichoderma reesei fungus (Rantanen et al. 2015). The activity properties of the enzyme are reported to be 17,700 nkat cm^{-3} cellulase with a protein level of 93 mg cm^{-3}

(Willberg-Keyriläainen et al. 2019). An amount of 3 mg of enzyme per gram of pulp fibre was added to a 2.5 w/w% suspension and the temperature was increased to 57 °C at pH 5.5 during hydrolysis, whilst keeping under constant agitation. The period of digestion was increased for each subsequent sample in 30 min steps, Table 1. The enzymatic activity was terminated by adjusting the pH to 9–10 by sodium carbonate and increasing the temperature to 90 °C. After cooling the suspension overnight in cold storage, the samples were refined using an homogeniser (model M-110P, Microfluidics, USA), passing the material under a pressure of 2000 bar through a 100 µm flow gap. The solids content of the MNFC suspension after the fluidisation was 1.65 w/w%.

The enzymatic pretreatment of pulp as a route for producing low-charged MNFC resulted in the production of short fibrils, which, in the case studied here, have much lower aspect ratio than MFC and NFC produced via chemical oxidative pretreatment or mechanical refining alone, as illustrated in Fig. 1 comparing MNFC/300/and MNFC/0/suspensions (Table 1), revealing much shorter fibrils obtained upon 300 min of enzymatic hydrolysis.

MNFC film preparation

With increasing enzymatic treatment time, the resulting MNFC suspension viscosity decreased significantly, and the solid content for preparation of the respective films ranged from 0.6 to 1.9 w/w% to meet the target film grammage of 60 g m^{-2} produced under conditions of 23 °C and relative humidity (RH) 50%.

Films were made on a sheet-former according to ISO standard 5269-1, with some modification of the screen to aid fines retention. Due to the very strong water retention of MNFC, and its fine size, a polyamide monofilament open mesh fabric SEFAR NITEX® 03-1/1 with a pore size of 1 µm was placed on top of a 125 µm metal screen. The pulp suspension was poured at high viscosity onto the former without adding water or stirring the slurry. The system was pressurised to 0.3 bar and the sealing lid was used on the sheet-former. Double-sided adhesive tape, of 5 mm width, was attached to the edges of the drying plate between plate and formed film, with purpose of fixing the edge of the film to prevent it shrinking during drying (Fig. 2).

Material treatment and characterisation

Optical microscopy was used to study the fibrillar sample suspensions and films using an Olympus BX 61 microscope equipped with a DP12 camera.

Water retention the water retention value (WRV) of the MNFC was determined in accordance to the standard SCAN-C 102XE with a slight modification in that 10 w/w% suspension of the MNFC was added in various ratios to a suspension of bleached unrefined pulp. The pulp matrix helps the MNFC dewater and remain retained on the screen. The WRV of neat MNFC can be evaluated by extrapolating to zero pulp, not including the swelling of the pulp fibres (Möller et al. 2010). The experiment was performed in triplicate for each sample.

Dielectric barrier discharge (DBD) plasma operates in a thermodynamically non-equilibrium condition (so-called cold plasma) in which the ion and molecular translational temperature is much lower than the electron temperature, such that excessive gas heating can be suppressed (Kostic et al. 2009; Prysiazhnyi et al. 2013). The advantage is that the plasma can be generated at atmospheric pressure, either in open or closed environment. In an open atmosphere, the plasma discharges can be produced with a gas flow between the electrodes (Mihailovic et al. 2011; Chu et al. 2002; Jens et al. 2017).

Table 1 Materials used in this study: bleached hardwood Kraft pulp treated with enzymes under controlled conditions, with progressive increase in enzymatic digestion time by 30 min steps for each subsequent sample

Enzymatic treatment time/min	0 (reference)	30	60	90	120	150	180	210	240	270	300
Sample label	MNFC/0/	MNFC/30/	MNFC/60/	MNFC/90/	MNFC/120/	MNFC/150/	MNFC/180/	MNFC/210/	MNFC/240/	MNFC/270/	MNFC/300/

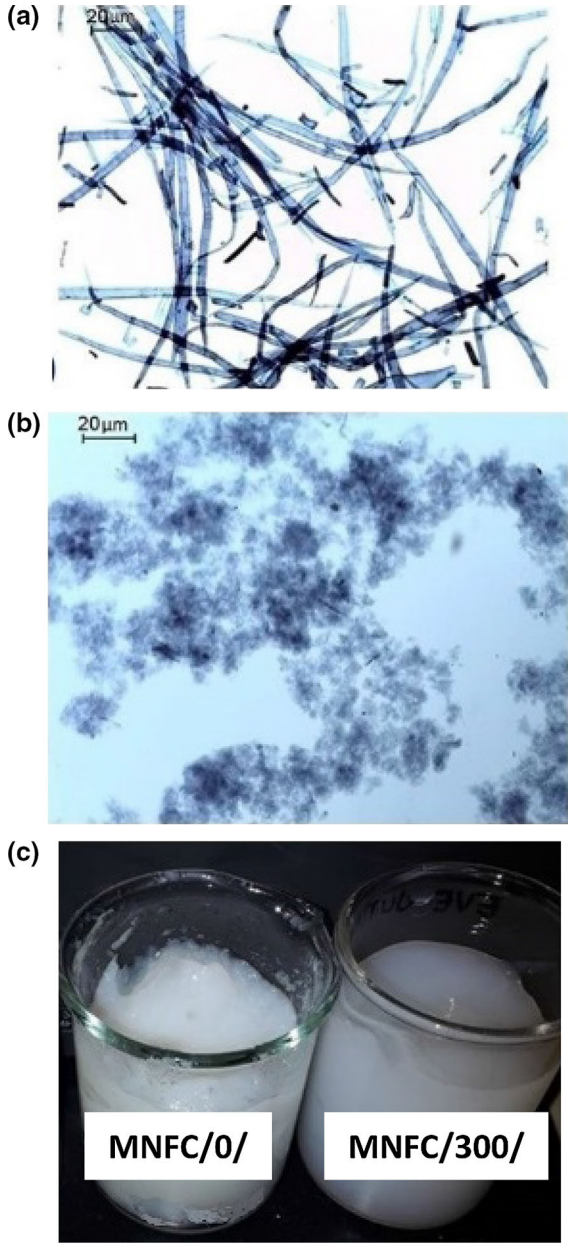

Fig. 1 Images of fibrils sample suspensions obtained with optical microscopy revealing the effect of processing conditions on the fibril size and aspect ratio: **a** without enzymatic treatment produced MNFC/0/yielding long fibrils, **b** MNFC/300/short, low aspect ratio fibrils, and **c** displaying the corresponding 2 w/w % MNFC suspensions of MFC/0/and MNFC/300/. The difference in gelation strength is due to the different size of fibrils and corresponding amount of water dispersed within the fibrillar matrix

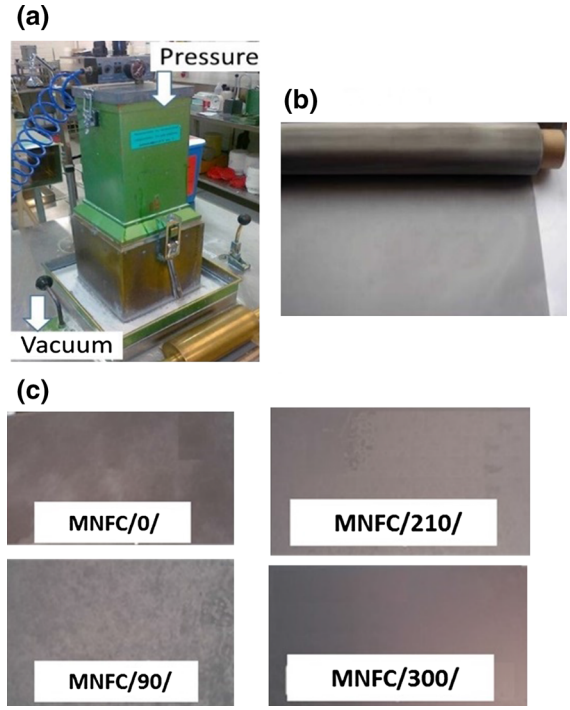

Fig. 2 MNFC film preparation: **a** sheet forming device with **b** 10 µm mesh supplemented nylon screen, and **c** samples of cut-offs (60 × 15 mm^2) from MNFC films produced from pulp refined with different enzymatic pretreatment time (Table 1). Transparency and uniformity of films increases with hydrolysis time

A further attractive characteristic of the DBD plasma at atmospheric pressure is that it can be used to modify or activate surfaces of a wide range of materials, from polymers, textile fibres to biological tissues, without damaging them (Kostic et al. 2009; Pertile et al. 2010; Mihailovic et al. 2011). To generate the DBD plasma we used a home-made device built at the Faculty of Physics, University Belgrade, Fig. 3. The DBD is assembled in a chamber with nitrogen gas injected into the discharge volume (6 dm^3 min^{-1}) through ten equidistant holes to ensure homogeneous gas flow. MNFC films were treated for 0 s, 30 s and 60 s, respectively. The device was operated at 6 kV DC and 300 electric field pulses per second (Hz) for the prescribed durations of time, for all the films, as a higher voltage resulted in burning of the thin MNFC films, especially for those made from pulp exposed to long enzymatic pretreatment time.

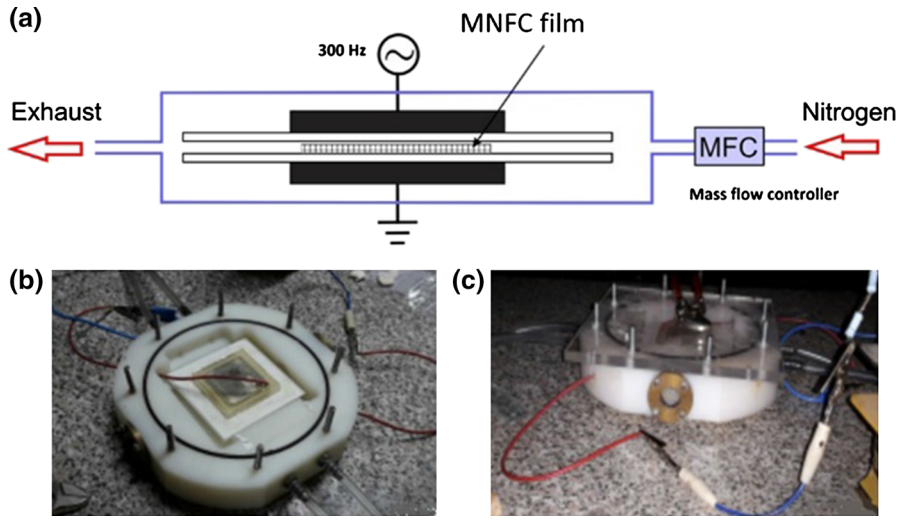

Fig. 3 DBD device with two electrodes and sample placed between them: **a** schematic illustration of DBD plasma devise, **b** plasma chamber housing the sample placed 1 mm from the upper electrode, and **c** closed plasma set up with glass lid placed above the top of the upper electrode

Determination of free surface energy (FSE) components

For the evaluation of any change in free surface energy of MNFC films arising from nitrogen plasma treatment, the contact angle (CA) is determined.

Most liquids are rapidly spreading on a high energy surface, and so a representative contact angle (CA) cannot be readily measured, Schultz et al. (1977) developed a method where CA can be measured by submerging the surface in one liquid and using a second liquid to measure the contact angle. In this case a hydrocarbon *n*-hexadecane is used as the submerging liquid having the purely dispersive liquid–vapour surface tension of $\gamma_{LV}^{h} = 27.4$ mJ m^{-2}, much lower than the expected surface free energy of the MNFC samples, and water as the contact angle liquid with the highly polar liquid–vapour surface tension $\gamma_{LV}^{w} = 72.8$ mJ m^{-2} (Hansson et al. 2011). A sessile drop of water is lowered into contact with the horizontal film immersed under hexadecane using a precise pipette delivering 70 µl of liquid and the progressive change in drop shape due to the change in CA recorded with a Nikon camera (D5000) in time steps of 1 ms. The CA of water is also recorded separately to represent the print challenge of a highly polar ink (Özkan et al. 2016; Dimic-Misic et al. 2015). For each given MNFC sample and given liquid data variation is within 10%. The identification of contact line geometry and evaluation of CA uses numeric software tools, as presented visually in Fig. 4. For a parallel optimal method for polar FSE determination with water alone, the Girifalco and Good approach (1957), combined with the Neumann equation of state was used. This latter allowed the polar contribution to FSE be estimated and thus can be added to the formerly measured dispersive component. Each measurement was conducted five times. For each given MNFC sample, the relative error of measured FSE was shown to be $\sim$ 10%.

Surface topography

Plasma action on the film surface can lead to a degree of debonding of fibrils as well as electrostatic charging and potential for subsequent additional moisture adsorption. Such changes can lead to re-conformation of the surface, even though no mechanical forces have been applied (Kostic et al. 2009; Chu et al. 2002). The change in topography of the MNFC films was investigated by Atomic Force Microscopy (AFM) (Veeco Instruments, model Dimension V). Using a MultiMode 8 with Bruker NanoScope V controller. Each MNFC film sample was dry-cast onto a Mica support for AFM imaging. Micrographs were obtained in trapping mode under ambient conditions, using TAP 300 tips (resonant frequency 300 kHz, line force being kept constant at 40 Nm^{-1} and the AFM images were processed and analysed with the Bruker NanoScope Analysis 1.5 software.

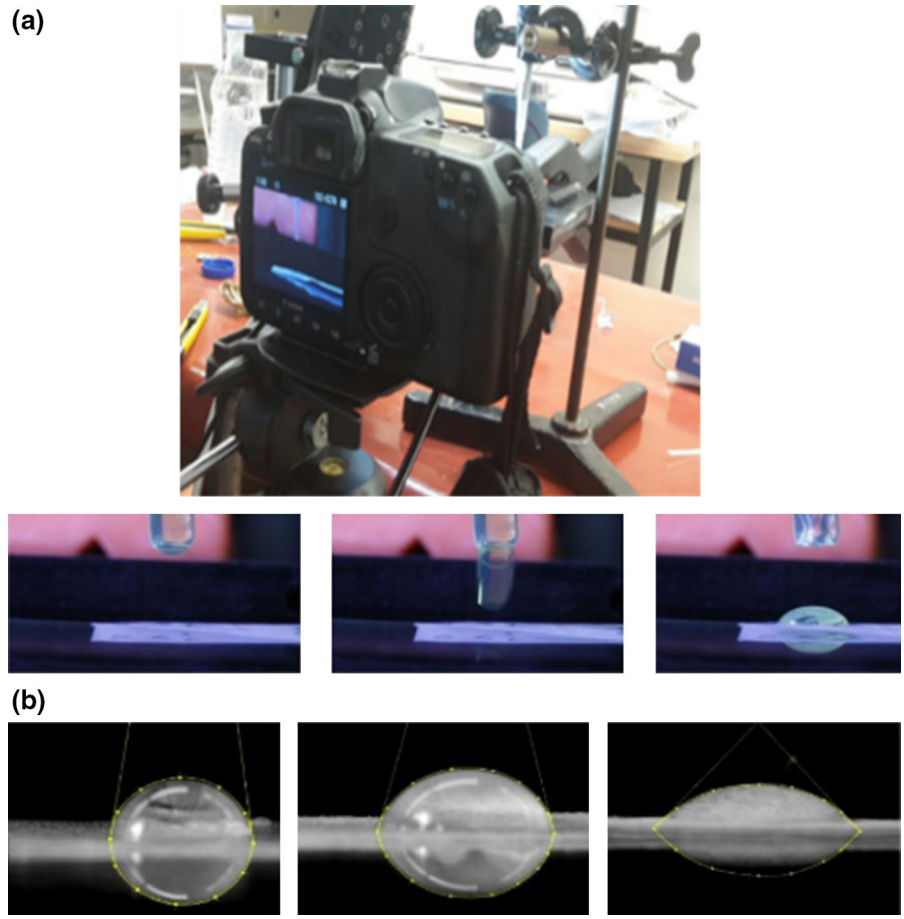

Fig. 4 Set-up for evaluating water CA under *n*-hexadecane with high speed camera (Nikon D5000): **a** images of films on camera viewfinder and **b** image processing of drop spreading (see also Fig. 8)

Mechanical properties

Mechanical properties of the MNFC films were measured by an MTS 400/M vertical tensile tester equipped with a 20 N load cell. The instrument was controlled by a TestWorks 4.02 program. Specimen strips with dimensions of 60 × 15 mm^2 were clipped from the MNFC films with a lab paper cutter (Afsahi et al. 2018). The thickness of the strips was separately measured with an L&W micrometer SE 250. The gauge length was 40 mm and the testing velocity was 0.5 mm min^{-1}. The results are presented as an average value obtained from five parallel specimens.

Surface chemical composition

Surface composition of the MNFC films was evaluated with X-ray photoelectron spectroscopy (XPS), using a Kratos AXIS Ultra electron spectrometer, with monochromatic Al Kα irradiation at 100 W and under charge neutralisation. Both the untreated MNFC films and plasma treated specimens were analysed. For the preparation, samples were pre-evacuated for at least 12 h, after which wide area survey spectra (for elemental analysis) as well as high resolution regions of C1*s* and O1*s* were recorded from several locations, and an in situ reference of pure cellulose was recorded for each sample batch (Johansson and Campbell 2004). With the parameters used, XPS analysis was recorded on an area of 1 mm^2 and the analysis depth is less than 10 nm. Carbon high resolution data were fitted using CasaXPS and a four component Gaussian fit tailored for celluloses.

MNFC suspension rheology

The rheological properties of MNFC suspensions were analysed at 2 w/w% concentration at 23 °C with an Anton Paar MCR 300 shear rheometer. The dynamic viscosity (η) was determined by steady shear-flow measurements, using the bob-in-cup geometry (Mohtaschemi et al. 2014). Due to the potential for wall depletion (apparent slip) and thixotropic behaviour of MNFC suspensions, the "bob" was a four-bladed vane spindle with a diameter of 10 mm and a length of 8.8 mm, while the metal cup had a diameter of 17 mm. A pre-shear protocol was applied using constant shear at a shear rate $\dot{\gamma}$ = 100 s^{-1} for 5 min, followed by a rest time of 10 min prior to recording the flow curves. Flow curves of MNFC suspensions were constructed under decreasing shear rate of $\dot{\gamma}$ = 1000–0.01 s^{-1}, with a logarithmic spread of data points (Dimic-Misic et al. 2013). To distinguish the MNFC suspensions in terms of their colloidal interactions as an effect of hydrolysis time, aspect ratio, crystallinity and friction between nanofibrils during the flow (Pääkkönen et al. 2016; Dimic-Misic et al. 2018), the log–log plot flow curves were fitted to a power law according to the Oswald–de Waele empirical model, as shown in Eq. (1)

$$\eta = k\dot{\gamma}^{1-n} \tag{1}$$

where k and n are the flow index and the power-law exponent, respectively: $n = 1$ indicates a Newtonian fluid and $n > 1$ indicates pseudo-plastic (shear thinning) behaviour.

The Herschel–Bulkley equation describes the dynamic yield stress τ_d^0 as

$$\tau = \tau_d^0 + k\dot{\gamma}^n \tag{2}$$

where τ is the shear stress.

Printing

The photovoltaic (PV) inkjet printing inks (IP) contain a complex mix of materials, solvent and surfactants that keep the p-type and n-type components de-mixed (Hashmi et al. 2015; Özkan et al. 2016). A piezoelectric laboratory scale drop-on-demand (DoD) materials inkjet printer (Dimatix 2831-DMP) was used to test the printability of the plasma treated MNFC films (Dimic-Misic et al. 2015). The solvent of the IP ink is 3-methoxypropionitrile, which is highly polar and non-volatile (boiling point 164 °C), viscosity 1.2 mPa s and density 0.937 g cm^{-3}, as stated by the supplier, Sigma Aldrich. The surface tension measurement was performed on the ink with an optical tensiometer (CAM 200 from KSV instruments) in pendant drop mode, giving a value of 29.2 mN m^{-1} (mJ m^{-2}).

Results and discussion

The *rheological properties* of the MNFC suspensions are given in Table 2, showing the change in dewatering, dynamic yield point and flocculation/water trapping gel-like structure (consistency coefficient, k) and shear thinning properties (index, n, expressed as the positive difference $n - 1$) and change in fibre morphology expressed as the fines content using the dynamic drainage jar (DDJ).

It is clear to see that with increase in enzymatic hydrolysis time, dewatering decreases as fibrils become thinner and smaller, and suspensions become more gel-like rheologically (Rantanen et al. 2015). At the same time, crystallinity of fibrils increases and water trapping structure/flocculation within the matrix with contrasting increased mobility in the flow regime once the structure is broken (Pääkkönen et al. 2016). The dynamic yield point, the minimum stress needed to be induced to set the suspension into flow increases as the suspensions become more gel like, but, also, breakage of that suspension induces greater shear thinning as fibrils are smaller and more crystalline, orienting easily in the flow direction (Pääkkönen et al. 2016; Hubbe et al. 2017b).

The *mechanical and optical* properties of MNFC films are presented in Table 3, where it is evident that the sheet density of the films increases with increase in hydrolysis time, while the packing density of the smaller crystalline particles increases. The permeability of those films created with the finer nanofibrils obtained after 120 min hydrolysis in turn falls rapidly, and it was not possible to measure using air flow techniques. The light scattering coefficient decreases also as the packing density is increased and the amorphous parts of the cellulose fibres were reduced, while, due also to higher packing density, the elasticity modulus increases, showing that films had improved strength.

Table 2 Properties of MNFC suspensions

Enzymatic treatment time (min)	WRV ($cm^3\ g^{-1}$)	Yield point, τ_d^0 (Pa)	Consistency coefficient, k (Pa s^{-n})	Shear thinning coefficient, $\|(1-n)\|$	DDJ fines value (%)
MNFC suspension properties					
0	1.25	34.12	431.23	0.82	93.8
30	1.61	47.34	241.3	0.81	88.8
60	1.83	54.23	139.65	0.81	79.5
90	2.19	68.45	89.67	0.81	62.4
120	2.55	91.45	69.45	0.84	27.0
150	2.85	438.34	57.23	0.84	21.0
180	2.98	29.82	35.15	0.86	11.8
210	3.33	19.64	19.67	0.86	9.6
240	3.37	12.67	14.34	0.87	6.5
270	3.32	8.99	9.97	0.89	1.5
300	3.34	4.74	5.45	0.91	0.2

Table 3 Mechanical and optical properties of MNFC films

Enzymatic treatment time (min)	Film weight ($g\ m^{-2}$)	Density ($g\ cm^{-3}$)	Permeability [$\mu m(Pa\ s)^{-1}$]	Light scattering coefficient ($m^2\ kg^{-1}$)	E-Modulus (GPa)
Film properties					
0	73.91	0.637	69.86	37.43	2.53
30	76.12	0.794	9.96	22.83	4.16
60	71.35	0.910	1.06	16.12	5.12
90	72.31	1.016	NA	9.94	7.02
120	70.53	1.090	NA	6.93	8.59
150	70.81	1.127	NA	5.81	9.13
180	69.57	1.145	NA	4.48	8.95
210	71.08	1.178	NA	3.74	11.26
240	70.10	1.179	NA	3.08	9.17
270	71.18	1.226	NA	3.11	9.76
300	65.27	1.187	NA	3.31	10.03

Roughness colour contour and profile plots of the surface of MNFC/30/150/300 films before and after plasma treatment are presented in Fig. 5. Before plasma treatment, the roughness of the films is directional, being different in in the two measured directions (red and blue profile lines). The map for MFC/30/indicates that there are voids present between 1 and 2 μm wide, while in the case of MFC/300/the surface is flatter with less voids and of much smaller size. This means that the degree of enzyme hydrolysis directly increases the resulting smoothness due to the ever finer fibrillar elements produced, as the crystalline parts are separated due to breakdown of the amorphous constituent. After plasma treatment, the amorphous material containing surfaces, e.g. MNFC/30/, are also seen to become relatively rougher than the highly hydrolysed crystalline films, e.g. MNFC/300/. The action of the plasma is to increase voyage in the courser particulate systems, as previously described, due to effects of charge, fibril debonding etc. (Jun et al. 2008). In MNFC/30/, it is possible to identify irregular both small and large voids appearing after plasma

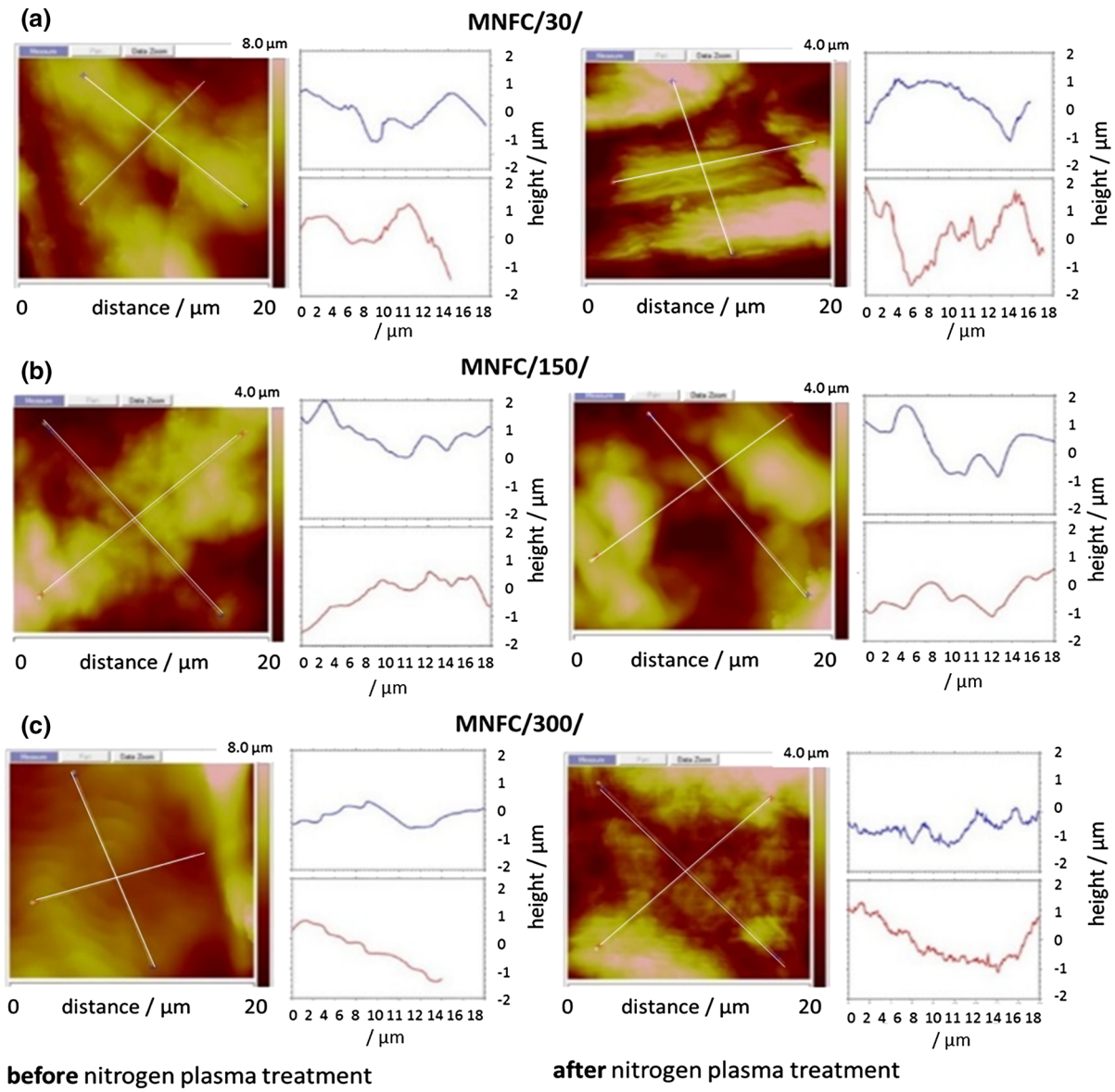

Fig. 5 Surface morphology and roughness of **a** MNFC/30/, **b** MNFC/150/ and **c** MNFC/300/before and after DBD nitrogen plasma treatment

treatment, while in MNFC/300/, the surface of the film has almost no such jagged appearance with voids only smaller than 1 µm. Nitrogen plasma treatment, thus, obviously changes the morphology of the films, on both the micro (nano) and macro level, which is likely also to have an influence on the wetting behaviour and decrease in CA due to the increased meniscus liquid–solid wetting line length (Prysiazhnyi et al. 2013; Pertile et al. 2010).

The *surface chemical species* are revealed by the XPS spectra, from which the atomic % of C–C, C–O, O–C=O and N can be derived, Fig. 6. The effect of surface modification after nitrogen plasma can be clearly seen as the level of N attachment increasing as a function of the enzymatic removal of amorphous content (Johansson and Campbell 2004). The samples with increased crystalline proportion after longer enzymatic treatment nonetheless show similar C–C bond content. Similarly, with reduction of the

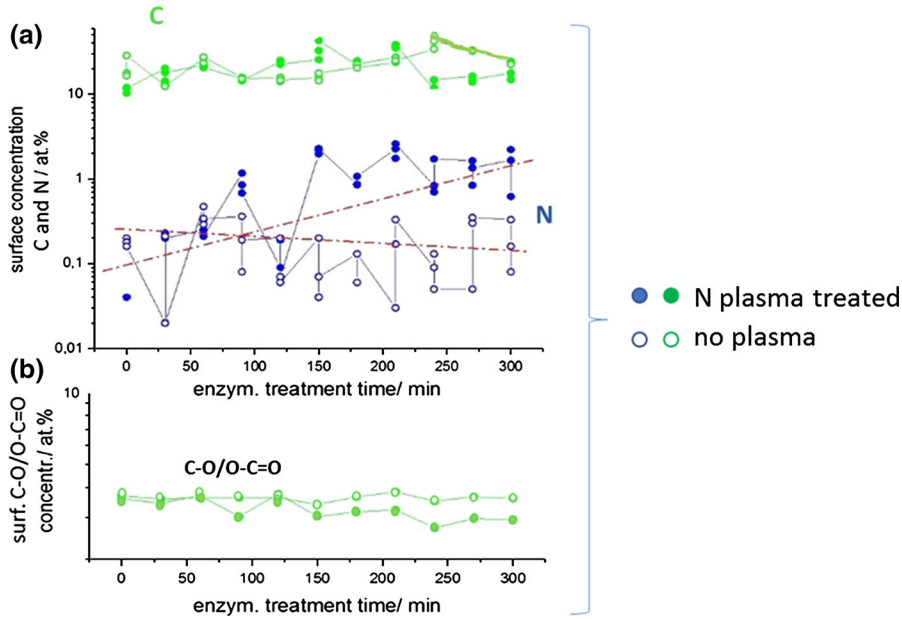

Fig. 6 Surface modification obtained through XPS data showing **a** increase in N atoms at constant carbon content, and **b** change in ratio of C–O/O–C=O groups

amorphous part with increased hydrolysis, the number of C–O groups decreases while C=O groups and other C and N containing groups are formed.

The results shown in Fig. 7 reveal that with the increase in enzymatic treatment of the raw material pulp there is a reduction of total FSE in the corresponding MNFC films in both polar and dispersive energy (green and blue unfilled symbols, respectively). A reversal of the decline in FSE as a function of enzymatic treatment can be observed resulting from nitrogen plasma treatment, showing compensating increases in both polar and dispersive measured components (green and blue filled symbols, respectively). Thus, an increase in wettability for water and n-hexadecane is reflected by a decrease in CA as the plasma treatment acts on the more crystalline samples (Johansson and Campbell 2004). However, as the roughness is also seen to increase as a function of plasma treatment for the lower crystalline samples (less exposure to enzymatic breakdown), one would expect from the Wenzel model that the wettability would increase. That we see a recorded increase in n-hexadecane CA, and thus decrease in dispersive FSE, we can conclude that the action of the plasma

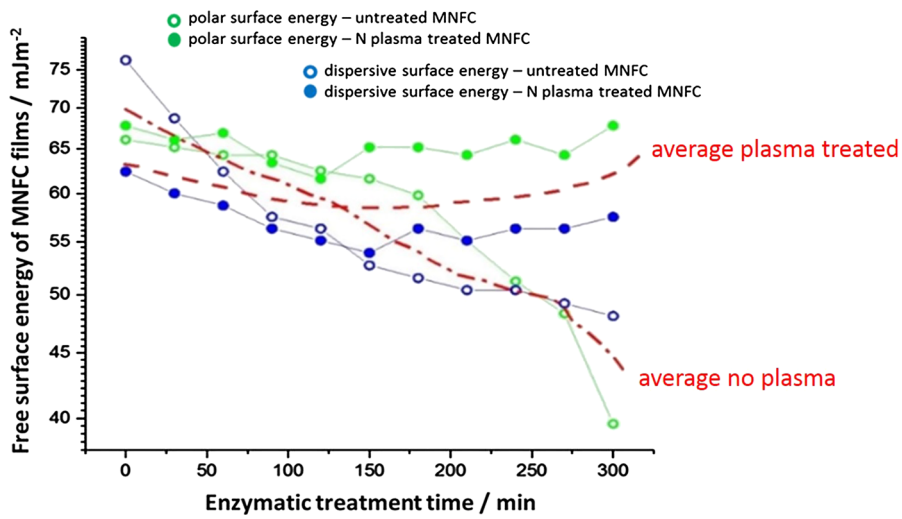

Fig. 7 Surface free energy (SFE) of MNFC films as a function of the treatment time (Table 1)

discharge on the amorphous part is initially to reduce the dispersive energy component, and so likely act, at least partially, to breakdown first the amorphous content resulting in debonding and hence roughening (Hansson et al. 2011). This effective etching of amorphous parts of fibrils is then replaced by the action of nitrogen attachment, such that the higher average FSE values regained in the more crystalline samples after plasma treatment are significantly higher than the theoretical FSE 59.4 mJ m^{-2} of cellulose, and this is achieved via the major contribution of the plasma-induced increase in polar component.

The increased contribution of the polar component in the FSE donated by the cationic N adsorption under plasma exposure is, therefore, expected to enhance the compatibility with the application of highly polar inks, especially if their components are anionic (Vanneste et al. 2017; Ma et al. 2010; Hoth et al. 2008). The images in Fig. 8 confirm this expectation, where the improved wetting of the surface by water as a function of plasma exposure time is paralleled by the greater pick-up (trapping) of ink colorant (Hoeng et al. 2016).

Summary and conclusions

Micro nanofibrillated cellulose films formed from aqueous suspension can be made stronger by pretreatment of the raw fibre using enzymatic hydrolysis. However, the wettability by ionic liquids, including functional inkjet printing inks, such as are suitably used for printed electronics, solar cells etc., decreases as a result, limiting the use of such films in practice. Nitrogen plasma treatment, however, enables wettability by such formulations to be improved. The mechanism by which this occurs has been studied in this work presented in this paper and the following conclusions can be drawn:

- Total free surface energy increases with nitrogen plasma treatment of highly enzymatically hydrolysed fibrillar films (contact angle decreases), with a major increase in the polar component.
  - Nitrogen is also included into the surface.
- Upon exposure to nitrogen plasma, dispersive surface energy initially decreases on those films made of pulp that was not treated or undergone short enzymatic treatment time, whereas the polar surface energy component remains relatively unchanged on such films.
  - This effect is related to the interaction of the nitrogen plasma with the amorphous cellulose component in the non-hydrolysed fibrils.
  - The dispersive energy component can once again be increased by exposure to nitrogen plasma in the case of the more crystalline fibrillar material derived from increased hydrolysis via enzymatic pretreatment.
- The surface area per unit mass was increased by the plasma treatment, apparently due to increased roughness on a nanometre scale.
- Highly ionic liquids, water and solvents typically used to disperse surfactant-containing organic-

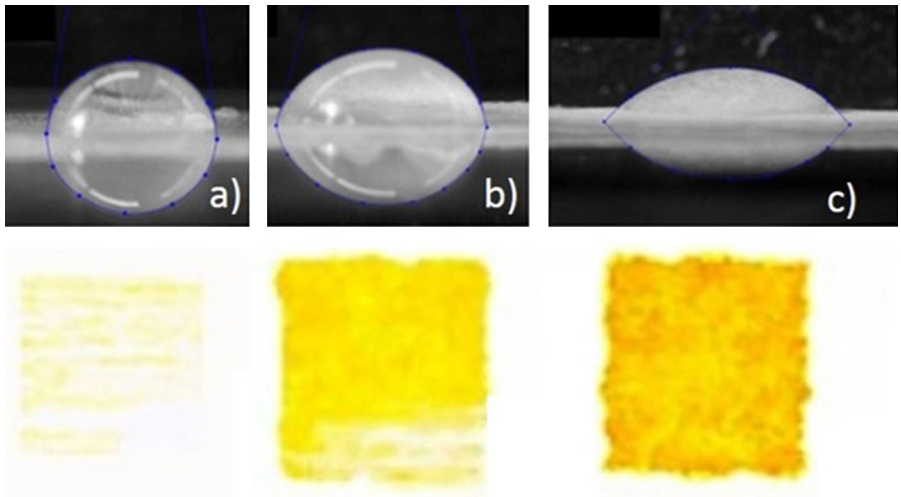

Fig. 8 IP ink printed on MNFC/300/film showing the dependence on wettability of the surface after nitrogen plasma treatment (see also Fig. 4); lower water droplet CA on the film corresponds with a significant increase in print colour density: **a** untreated film, **b** plasma treated for 30 s and **c** plasma treated for 60 s

based inks, wet MNFC film better as hydrolysing pretreatment of fibres is increased and subsequent nitrogen plasma is applied.

Perspectives and future work arising from these findings include the need to study the origins of the surface roughening effect. Is this a random generation of surface disruption or is there a material transfer mechanism at play, involving perhaps vaporisation and redisposition? The impact on the amorphous component by plasma treatment could offer a means to induce a phase change at the material surface. Similarly, other gas plasma treatments should be investigated in the longer term to understand whether the role of atomic substitution versus the application of energy discharge has the greater treatment potential.

Acknowledgments Open access funding provided by Aalto University. The authors from the Institute of Physics Belgrade gratefully acknowledge financial help from the Ministry of Education, Science and Technological Development of the Republic of Serbia. The authors wish to thank to Prof. Milorad M. Kuraica from the Faculty of Physics, Laboratory for Plasma Physics, University of Belgrade, for his patience and skill in assisting with plasma experiments. Open access funding provided by Aalto University.

References

Afsahi G, Dimic-Misic K, Gane P, Budtova T, Maloney T, Vuorinen T (2018) The investigation of rheological and strength properties of NFC hydrogels and aerogels from hardwood pulp by short catalytic bleaching (H cat). Cellulose 25:1637–1655

Catia R, Castro G, Rana S, Fangueiro R (2015) Characterization of physical, mechanical and chemical properties of quiscal fibres: the influence of atmospheric DBD plasma treatment. Plasma Chem Plasma Process 35:863–878

Cernakova L, Stahel P, Kovacik C, Johansson K, Cernak M (2006) Low-cost high-speed plasma treatment of paper surfaces. In: 9th TAPPI advanced coating fundamentals symposium, Turku, Finland, pp 8–10

Chu PK, Chen JY, Wang LP, Huang N (2002) Plasma-surface modification of biomaterials. Mater Sci Eng R Rep 36:143–206

Dimic-Misic K, Puisto A, Gane P, Nieminen K, Alava M, Paltakari J, Maloney T (2013) The role of MFC/NFC swelling in the rheological behaviour and dewatering of high consistency furnishes. Cellulose 20:2847–2861

Dimic-Misic K, Karakoc A, Özkan M, Ghufran HS, Maloney T, Paltakari J (2015) Flow characteristics of ink-jet inks used for functional printing. J Appl Eng Sci 13:207–212

Dimic-Misic K, Maloney T, Gane P (2018) Effect of fibril length, aspect ratio and surface charge on ultralow shear-induced structuring in micro and nanofibrillated cellulose aqueous suspensions. Cellulose 25:117–136

Galagan Y, Rubingh JEJ, Andriessen R, Fan CC, Blom PW, Veenstra SC, Kroon JM (2011) ITO-free flexible organic solar cells with printed current collecting grids. Solar Energy Mater Solar Cells 95:1339–1343

Girifalco LA, Good RJ (1957) A theory for the estimation of surface and interfacial energies. I. Derivation and application to interfacial tension. J Phys Chem 61:904–909

Hansson PM, Skedung L, Claesson PM, Swerin A, Schoelkopf J, Gane PAC, Rutland MW, Thormann E (2011) Robust hydrophobic surfaces displaying different surface roughness scales while maintaining the same wettability. Langmuir 27:8153–8159

Hashmi SG, Özkan M, Halme J, Dimic-Misic K, Zakeeruddin SM PJ, Grätzel M, Lund PD (2015) High performance dye-sensitized solar cells with inkjet printed ionic liquid electrolyte. Nano Energy 17:206–215

Hoeng F, Denneulin A, Bras J (2016) Use of nanocellulose in printed electronics: a review. Nanoscale 8:13131–13154

Hoth CN, Schilinsky P, Choulis SA, Brabec CJ (2008) Printing highly efficient organic solar cells. Nano Lett 8(2008):2806–2813

Hubbe MA, Ferrer A, Tyagi P, Yin Y, Salas C, Pal L, Rojas OJ (2017a) Nanocellulose in thin films, coatings, and plies for packaging applications: a review. BioResources 12:2143–2233

Hubbe MA, Tayeb P, Joyce M, Tyagi P, Kehoe M, Dimic-Misic K, Pal L (2017b) Rheology of nanocellulose-rich aqueous suspensions: a review. BioResources 12:9556–9661

Jens V, Ennaert T, Vanhulsel A, Sels B (2017) Unconventional pretreatment of lignocellulose with low-temperature plasma. Chemsuschem 10:14–31

Johansson LS, Campbell JM (2004) Reproducible XPS on biopolymers: cellulose studies. Surf Interface Anal 36:1018–1022

Jun W, Fengcai Z, Bingqiang C (2008) The solubility of natural cellulose after DBD plasma treatment. Plasma Sci Technol 10:743

Jutila E, Koivunen R, Kiiski I, Bollström R, Sikanen T, Gane PAC (2018) Microfluidic lateral flow cytochrome P450 assay on a novel printed functionalized calcium carbonate-based platform for rapid screening of human xenobiotic metabolism. Adv Funct Mater 28(31):1802793–1802803

Kostić M, Radić N, Obradović BM, Dimitrijević S, Kuraica MM, Škundrić P (2009) Silver-loaded cotton/polyester fabric modified by dielectric barrier discharge treatment. Plasma Process Polym 6(1):58–67

Kramer F, Klemm D, Schumann D, Heßler N, Wesarg F, Fried W, Stadermann D (2006) Nanocellulose polymer composites as innovative pool for (bio) material development.

In: Macromolecular symposia, WILEY-VCH Verlag, vol 244, pp 136–148

Kumar P, Chand S (2012) Recent progress and future aspects of organic solar cells. Prog Photovolt Res Appl 20:377–415

Ma H, Yip HL, Huang F, Jen AKY (2010) Interface engineering for organic electronics. Adv Funct Mater 20:1371–1388

Maloney TC (2015) Network swelling of TEMPO-oxidized nanocellulose. Holzforschung 69:207–213

Mihailović D, Šaponjić Z, Radoičić M, Lazović S, Baily CJ, Jovančić P, Nedeljković J, Radetić M (2011) Functionalization of cotton fabrics with corona/air RF plasma and colloidal TiO_2 nanoparticles. Cellulose 18:811–825

Mohtaschemi M, Dimic-Misic K, Puisto A, Korhonen M, Maloney T, Paltakari J, Alava MJ (2014) Rheological characterization of fibrillated cellulose suspensions via bucket vane viscometer. Cellulose 21:1305–1312

Möller M, Leyland N, Copeland G, Cassidy M (2010) Self-powered electrochromic display as an example for integrated modules in printed electronics applications. Eur Phys J Appl Phys 5:33205

Özkan M, Dimic-Misic K, Karakoc A, Hashm SG, Lund P, Maloney T, Paltakari J (2016) Rheological characterization of liquid electrolytes for drop-on-demand inkjet printing. Organ Electron 38:307–315

Pääkkönen T, Dimic-Misic K, Orelma H, Pönni R, Vuorinen T, Maloney T (2016) Effect of xylan in hardwood pulp on the reaction rate of TEMPO-mediated oxidation and the rheology of the final nanofibrillated cellulose gel. Cellulose 23(1):277–293

Pertile RA, Andrade FK, Alves JC, Gama M (2010) Surface modification of bacterial cellulose by nitrogen-containing plasma for improved interaction with cells. Carbohydr Polym 82:692–698

Prysiazhnyi V, Kramar A, Dojcinovic B, Zekic A, Obradovic BM, Kuraica MM, Kostic M (2013) Silver incorporation on viscose and cotton fibers after air, nitrogen and oxygen DBD plasma pretreatment. Cellulose 20:315–325

Rantanen J, Dimic-Misic K, Kuusisto J, Maloney TC (2015) The effect of micro and nanofibrillated cellulose water uptake on high filler content composite paper properties and furnish dewatering. Cellulose 22:4003–4015

Schultz J, Tsutsumi K, Donnet JB (1977) Surface properties of high-energy solids: II. Determination of the nondispersive component of the surface free energy of mica and its energy of adhesion to polar liquids. J Colloid Interface Sci 59:277–282

Singh M, Haverinen HM, Dhagat P, Jabbour GE (2010) Inkjet printing-process and its applications. Adv Mater 22:673–685

van de Vyver S, Geboers J, Jacobs PA, Sels BF (2011) Recent advances in the catalytic conversion of cellulose. ChemCatChem 3:82–94

Vanneste J, Ennaert T, Vanhulsel A, Sels B (2017) Unconventional pretreatment of lignocellulose with low-temperature plasma. ChemSusChem 10(1):14–31

Willberg-Keyriläainen P, Ropponen J, Lahtinen M, Pere J (2019) Improved reactivity and derivitization of cellulose after pre-hydrolysis with commercial enzymes. BioResources 14(1):561–574

Yinhua Z, Fuentes-Hernandez C, Khan TM, Liu JC, Hsu J, Shim JW, Dindar A, Youngblood JP, Moon RJ, Kippelen B (2013) Recyclable organic solar cells on cellulose nanocrystal substrates. Sci Rep 3:1536

Zhu H, Narakathu BB, Fang Z, Aijazi AT, Joyce M, Atashbar M, Hu L (2014) A gravure printed antenna on shape-stable transparent nanopaper. Nanoscale 6(15):9110–9115